

# In situ Ramsey Interferometry and Diffraction Echo with an Ultracold Fermi Gas

C. Marzok, B. Deh, S. Slama, C. Zimmermann, and Ph.W. Courteille  
*Physikalisches Institut, Eberhard-Karls-Universität Tübingen,  
Auf der Morgenstelle 14, D-72076 Tübingen, Germany*  
(Dated: November 9, 2018)

We report on the first observation of Bragg scattering of an ultracold  ${}^6\text{Li}$  Fermi gas. We demonstrate a Ramsey-type matter-wave interferometer based on Bragg diffraction and find robust signatures of persistent matter wave coherences using an echo pulse sequence. Because of the Pauli principle, the diffracted fermions oscillate nearly unperturbed in the trapping potential for long times beyond 2 s. This suggests extremely long coherence times. On these timescales, only the presence of a  ${}^{87}\text{Rb}$  cloud seems sufficient to induce noticeable perturbations.

PACS numbers: 03.75.Ss, 37.10.Jk, 37.25.+k, 67.85.Pq

Bragg diffraction of cold atoms off moving periodic optical potentials has been established as a standard tool for coherent atom optics since its first application to Bose-Einstein condensates (BECs) almost ten years ago [1]. Atoms moving with a wave vector fulfilling the Bragg condition scatter light from the copropagating into the counterpropagating laser beam and are accelerated by two photon recoil momenta. Bragg diffraction has extensively been used in a technique called Bragg spectroscopy [2] serving to measure the dispersion relation and the dynamic structure factor of BECs and molecular condensates [3] and to provide signatures of vortices [4]. For ultracold fermion gases, Bragg diffraction is expected to be able to reveal the pairing mechanism in the BEC-BCS crossover regime by measuring the dynamic structure factor for both density and spin [5].

Because Bragg diffraction coherently couples two momentum states, it is frequently used as a beamsplitter for matter waves in interferometric experiments. Such schemes have been applied to BECs [6], which bear the advantage of a macroscopically populated wavefunction yielding a high interferometric contrast. On the other hand, in BECs the typical lifetime of coherent superposition states is only on the order of  $10\ \mu\text{s}$  due to interatomic interactions. For Fermi gases the matter wave contrast is necessarily limited to single particle interference, because identical fermions cannot interfere. The advantage of ultracold spin-polarized Fermi gases is that they are interaction-free, so that coherent superpositions of motional states are expected to live very long. Coherence times of hundreds of milliseconds in superpositions of Wannier-Stark states in a vertical optical lattice have first shown the superiority of interaction free Fermi gases for interferometry [7].

This paper reports the first study of Bragg interferometry with ultracold fermionic spin polarized  ${}^6\text{Li}$  atoms inside a magnetic trap using a moving optical lattice. It turns out that the momentum distribution after diffraction periodically revives after multiples of the trap period for more than a hundred times. This suggests very long coherence times due to the absence of s-wave interactions. In contrast, the presence of interacting  ${}^{87}\text{Rb}$  atoms quickly damps out the revival. With a Ramsey

type Bragg pulse sequence, a matter-wave interferometer can be realized. At finite temperatures, atoms at different momenta are Doppler shifted which leads to a detuning of the interferometer for different momentum classes. A complete Ramsey spectrum can thus be recorded in a single shot. For long time intervals between the Ramsey pulses, however, the fringe spacing is beyond the resolution limit of the imaging system. In contrast to decoherence as in the case of interacting bosons, which irreversibly destroys quantum superpositions, dephasing can be reversed by an appropriate manipulation of the individual atomic phases. Rephasing of coherent superpositions of atomic excitations has been demonstrated in spin echo [8] as well as in photon echo [9]. Phonon echoes have been observed both in fused silica glasses [10] as well as in cold trapped atomic clouds [11]. We show that a tailored pulse sequence consisting of  $\frac{\pi}{2}-\pi-\frac{\pi}{2}$  pulses leads to an echo type revival of the diffraction pattern. In particular, echo diffraction patterns exhibits very robust signatures for the degree of coherence of momentum superposition states, allowing us to detect coherence times of at least  $100\ \mu\text{s}$  in the experiment. Furthermore, simulations show that such echo type experiments are sensitive to coherence times of seconds and longer, if the pulses are applied in a stroboscopic fashion after multiples of the trap oscillation period.

The cooling procedure we use for cooling a mixture of  ${}^6\text{Li}$  and  ${}^{87}\text{Rb}$  atoms has been reported in a previous paper [12]. In short, the two species are simultaneously collected by a magneto-optical trap and then transferred via several intermediate magnetic traps into a Ioffe-Pritchard type trap, where they are stored in their respective hyperfine states  $|3/2, 3/2\rangle$  and  $|2, 2\rangle$ . Two trap configurations are used in the experiment. The *compressed* trap is characterized by the secular frequencies  $(\omega_x, \omega_y, \omega_z)/2\pi = (762, 762, 190)$  Hz for  ${}^6\text{Li}$  and the magnetic field offset 3.5 G. For  ${}^{87}\text{Rb}$  the trap frequencies are  $\sqrt{87/6}$  times lower. The  ${}^{87}\text{Rb}$  cloud is selectively cooled by microwave-induced forced evaporation. The  ${}^6\text{Li}$  is sympathetically cooled via interspecies thermalization. For the experiments described below, we typically reach temperatures of a few hundred nK with  $2.3 \cdot 10^6$   ${}^{87}\text{Rb}$  atoms and  $\sim 1.2\ \mu\text{K}$  with  $2 \cdot 10^5$   ${}^6\text{Li}$  atoms. The  ${}^6\text{Li}$

does not reach the  $^{87}\text{Rb}$  temperature due to the smallness of the interspecies scattering length [12].

All experiments, unless stated otherwise, are carried out in a *decompressed* trap characterized by the secular frequencies  $(\omega_x, \omega_y, \omega_z)/2\pi = (236, \sim 180, 141)$  Hz for  $^6\text{Li}$ . In this trap, the different gravitational sagging of the  $^{87}\text{Rb}$  and  $^6\text{Li}$  clouds separates them in space. Consequently, the  $^6\text{Li}$  cloud does not thermalize and acquires an anisotropic momentum distribution upon decompression. For the  $z$ -axis we measure a momentum width corresponding to the temperature  $T_z \simeq 0.9 \mu\text{K}$ .

Bragg diffraction is performed using two laser beams counterpropagating along the  $z$ -axis and tuned  $\sim 1$  GHz to the red from the  $D_2$  line of  $^6\text{Li}$ . Their frequencies differ by an amount  $\delta = \omega_2 - \omega_1 = 2\hbar q^2/m = 2\pi \cdot 295$  kHz, where  $q = 2\pi/\lambda$ ,  $\lambda = 670.977$  nm and  $m$  is the atomic mass of  $^6\text{Li}$ . The lasers are phase-locked by means of an electronic feedback circuit. The Bragg beams have intensities  $I_1 = I_2 = 13.7 \dots 132$  mW/cm<sup>2</sup>, corresponding to one-photon Rabi frequencies of  $\Omega_i = \sqrt{6\pi c^2 \Gamma_i / \hbar \nu^3}$ , so that the two-photon Rabi frequency  $\Omega_R = \Omega_1 \Omega_2 / 2\Delta_L$  covers the range  $2\pi(47 \dots 450)$  kHz. In most experiments, before applying an in situ Bragg pulse (or a series of pulses), the  $^{87}\text{Rb}$  atoms are removed from the trap with a resonant light pulse. After the Bragg pulse, we wait for half an oscillation period to rephase the momentum distribution before we switch off the trapping field and map the momentum distribution after 2 ms of ballistic expansion by absorption imaging.

The second image of Fig. 1(a) shows a  $^6\text{Li}$  absorption image taken after application of a single Bragg pulse, whose length  $\tau$  corresponds to  $\Omega_R \tau \approx \pi/2$ . For low Rabi frequencies, only a narrow slice is cut out of the fermionic momentum distribution. The position of the slice along the  $z$ -axis depends on the detuning of the Bragg lasers from the two-photon recoil shift,  $\Delta = \delta - 2\hbar q^2/m$ , the width is due to power broadening by the Rabi frequency  $\Omega_R$ . When the pulse area is increased beyond  $\pi/2$ , the momentum distribution acquires a more complicated, axially modulated shape. This is due to the fact that the various momentum classes of the atomic cloud are Doppler detuned from the Bragg condition and therefore experience different effective Rabi flopping frequencies.

The experimental data can be well described by a theoretical simulation. Fig. 1(b,d). In our model we assume that for every atom the Bragg lasers couple only two discrete momentum states. The evolution of every momentum class is calculated individually from the Schrödinger equation. The sum of the results is weighted with the initial momentum distribution. In cases where the possibility of phase decoherence is considered, e.g. by interatomic interactions, we use a two-level Bloch equation model. As long as the evolution of the momentum distribution under the action of the trapping potential is not taken into account, the above treatment only applies to short pulse sequences,  $\tau \ll 2\pi/\omega_z$ , or to stroboscopic sequences that are synchronized with the trap period.

To study the impact of both the trap and of colli-

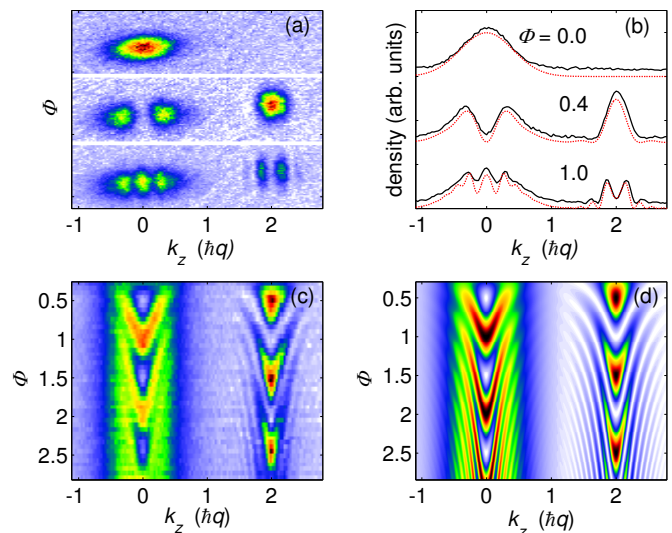


FIG. 1: (Color online) (a) Time-of-flight absorption images of a  $1 \mu\text{K}$  cold cloud after a single Bragg scattering pulse and a 2 ms ballistic expansion period. From the top to the bottom the Bragg pulse area is varied,  $\Phi \equiv \Omega_R \tau / 2\pi = 0, 0.4, \text{ and } 1$ . The experimental Rabi frequency is  $\Omega_R / 2\pi = 47$  kHz. The tilted shape of the diffracted clouds is due to alignment imperfection of the Bragg lasers with respect to the trap's weak axis. (b) The solid lines show the integration of the time-of-flight absorption images shown in (a) along the radial direction (perpendicular to laser's wavevectors). The dashed lines show simulations of the axial momentum distributions with no free parameters. (c) False color map of measured momentum distributions for pulse areas varied from 0 to  $5\pi$ . The radially integrated absorption images appear as rows. (d) False color map of the calculated momentum distributions using experimental parameters.

sions on the momentum distribution, we apply a single  $\pi$ -pulse, let the atoms oscillate in the trap for a long time  $t \gg 2\pi/\Omega_R$  and then image the cloud's momentum distribution. This experiment has been performed in the compressed trap, because in this configuration there is spatial overlap between  $^6\text{Li}$  and  $^{87}\text{Rb}$  clouds. By counting the numbers of atoms in a restricted area of momentum space corresponding to the first-order Bragg-diffracted atoms, we obtain the curves shown in Fig. 2(a) for the case of no  $^{87}\text{Rb}$  inside the trap. Apparently, the atoms oscillate more than a hundred times with only small damping corresponding to an exponential decay time of 2.4 s. This extremely long dephasing time impressively demonstrates that diffusion in momentum space is very slow [13]. As collisions, which are forbidden by the Pauli principle, are absent, momentum dephasing is mainly due to residual anharmonicities of the trapping potential. In this respect the Fermi gas efficiently emulates the dynamics of an ideal gas of non-interacting particles.

We tested the impact of collisions by keeping the  $^{87}\text{Rb}$  in the trap. For this case, Fig. 2(b) shows a dramatic reduction of the decay time for the  $^6\text{Li}$  cloud to 0.15 s. This value agrees well with the inverse collision rate esti-

ated for the densities and temperatures specified above.  $\gamma_{coll}^{-1} \simeq 0.16$  s [12, 14]. Thus, for the mixture, we expect coherent states to decay on this time scale. The exis-

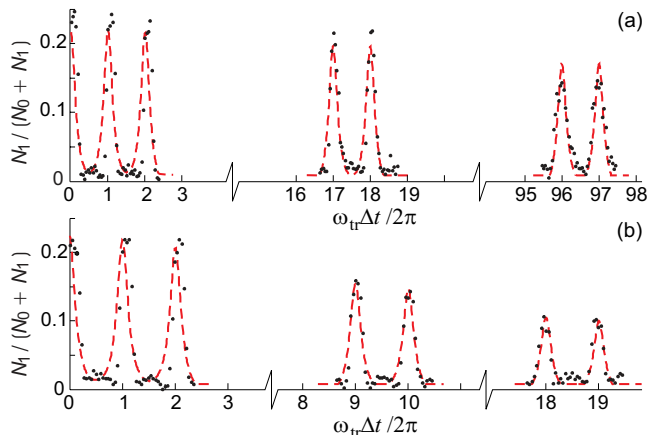


FIG. 2: (Color online) Rephasing of the momentum distribution in the trap in the absence (a) and in the presence (b) of  $^{87}\text{Rb}$ . The population of the state  $2\hbar q$  normalized to the total number of atoms in states  $0\hbar q$  and  $2\hbar q$ , denoted  $N_0$  and  $N_1$  respectively. The peaks represent full trap oscillations. The dashed line gives an array of Gaussian functions, whose amplitudes are decreasing exponentially in time. The fits to the data yield the decay times for (a) 2.4 s and for (b) 0.15 s. The oscillation frequency was  $\omega_z/2\pi = 142.51$  Hz and the Rabi frequency  $\Omega_R/2\pi = 47$  kHz.

tence and the lifetime of such states can be tested by interferometric experiments. Furthermore, they justify stroboscopic timing for absorption imaging and for interferometry.

To check the lifetime of coherent superpositions of momentum states, we apply a Ramsey sequence of two  $\pi/2$  Bragg pulses separated by a variable short time interval  $\Delta t \ll 2\pi/\omega_z$ . The inhomogeneous momentum distribution of the atoms corresponds to a Doppler-shift, which detunes the atoms from the resonant Bragg condition. Therefore, the atoms accumulate different phases during their free evolution in the trap, which allows to observe a full Ramsey spectrum in a single shot, as shown in Fig. 3. While we do observe Ramsey fringes for time intervals up to  $\Delta t \simeq 32 \mu\text{s}$ , for longer times, the fringe spacing is below the resolution limit of the imaging system. Lower temperatures improve the fringe contrast without influencing the fringe spacing. The resolution can also be somewhat enhanced by longer times of flight at the expense of contrast.

More robust signatures are needed to find out, whether coherence is preserved for times exceeding  $32 \mu\text{s}$ . A well-known method to rephase the momentum distribution and to obtain Doppler-free signals is echo interferometry [15]. This method divides the free evolution time in a Ramsey experiment in two periods separated by a  $\pi$ -pulse. The  $\pi$ -pulse inverts the accumulated phase delay of the different atomic momentum classes so that the states rephase during the time interval after the  $\pi$ -pulse.

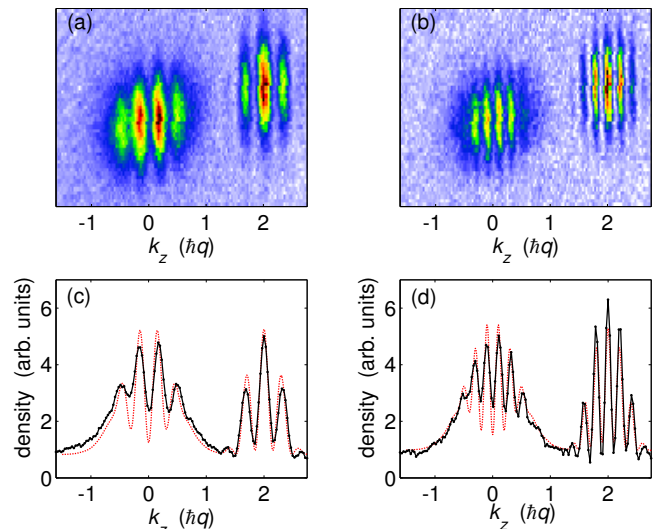


FIG. 3: (Color online) (a,b) Time-of-flight absorption images taken after a Ramsey pulse sequence and (c,d) their radial integrations (black solid line). The times between the Ramsey pulse are (a,c)  $6 \mu\text{s}$  and (b,d)  $12 \mu\text{s}$ . The theoretical curves (red dotted line) in (b,d) are fits based on our model.  $\omega_z/2\pi = 142.51$  Hz and  $\Omega_R/2\pi = 57$  kHz are as in Fig. 1.

Thus, all momentum classes contribute to the signal.

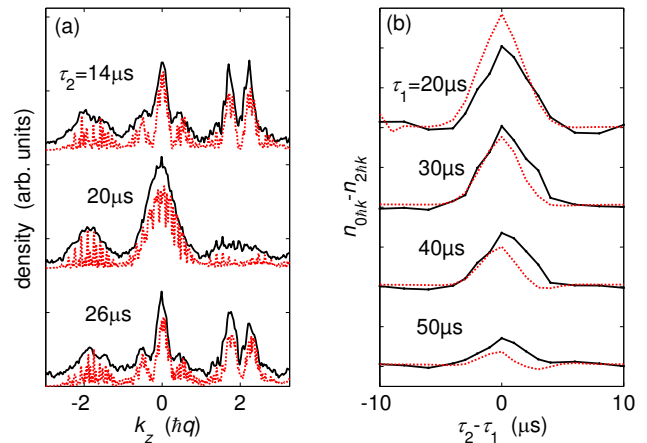


FIG. 4: (Color online) (a) Radially summed absorption images (black solid line) taken after an echo sequence  $\frac{\pi}{2} - \tau_1 - \pi - \tau_2 - \frac{\pi}{2}$  for  $\tau_1 = 20 \mu\text{s}$ . Also shown are simulated momentum distributions calculated with experimental parameters (red dotted line). (b) Difference of the measured (black solid line) and simulated (red dotted line) relative populations of the states  $k_z = 0\hbar q$  and  $k_z = 2\hbar q$  for varying  $\tau_2$  with different fixed values of  $\tau_1$ . The echo signal washes out for  $\tau_1$ -times larger than  $50 \mu\text{s}$ .

The momentum distributions observed after an echo sequence in the regime of *small* Rabi frequencies  $\Omega_R \ll \hbar k_{\text{th}}^2/2m$  exhibit a central dip for atoms near  $2\hbar q$ , whose width depends on  $\Omega_R$  (data not shown). Theoretical simulations show that low-energy atomic momentum classes, which are within the area of this dip are efficiently

rephased by the echo pulse scheme and the  $2\hbar q$  state is depopulated by the second  $\frac{\pi}{2}$ -pulse. For higher momenta, the Doppler-shift causes the pulse areas to deviate considerably from  $\frac{\pi}{2}$  which corrupts the echo rephasing scheme. Nevertheless, simulations reveal that the width of the dip is very stable even after long times  $\Delta t \gg 2\pi/\omega_z$ . In contrast, in the presence of decoherence, the dip vanishes. The appearance of the dip in the momentum profile thus represents a robust signature for coherence, preferable to Ramsey fringes as it overcomes limits in momentum resolution.

For *higher* Rabi frequencies, more atoms contribute to the echo signal, thus increasing the signal-to-noise ratio. For  $\Omega_R \geq \hbar k_{\text{th}}^2/2m$  the whole population of the momentum states has to be monitored. In Fig. 4, diffraction echo is demonstrated for  $\Omega_R/2\pi = 220$  kHz. A  $\frac{\pi}{2}$ - $\pi$ - $\frac{\pi}{2}$  pulse sequence with delay times of  $\tau_1$  and  $\tau_2$  between the pulses has been applied. In Fig. 4(a) diffraction echo manifests itself in an almost complete revival of the  $k_z = 0\hbar q$  momentum state when  $\tau_1 = \tau_2 = 20$   $\mu$ s. As is apparent in the data, the  $k_z = -2\hbar q$  state is also slightly populated as one approaches the crossover regime from Bragg scattering to Kapitza-Dirac scattering. An extended model including higher momentum states as well as trap oscillations successfully reproduces the measured momentum distributions (red dotted line). The initial spatial distribution is also taken into account for each  $k_z$  individually. The spikes in the model curve arise from the limited number of initial space coordinates used for averaging due to limitations in available computing power. Subtracting the population of state  $2\hbar q$  from state  $0\hbar q$  shows the quantitative effect of diffraction echo [Fig. 4(b)]. The echo signal fades out after 100  $\mu$ s. This is an effect of the spatial distribution and does not need decoherence for an explanation. The extended model predicts a revival of the echo signal for  $\tau_1 = \tau_2 = T_{\text{trap}} = 7.092$  ms, where  $T_{\text{trap}}$  is the trap period. Measurements have not shown such a revival, although we expect coherence to persist on this timescale. Possible technical reasons which could account for an incomplete refocussing of the atomic phases could be fluctuating Ramsey pulse lengths, power or frequency fluctuations of the Bragg lasers, or alignment imperfections of the Bragg beams with respect to the  $z$ -axis.

tuating Ramsey pulse lengths, power or frequency fluctuations of the Bragg lasers, or alignment imperfections of the Bragg beams with respect to the  $z$ -axis.

In conclusion, we studied the coherence lifetime of an ultracold Fermi gas via *in situ* Bragg interferometry. We demonstrated that the method of diffraction echo is capable of producing robust signatures of coherence, but is today limited by practical imperfections of the experimental setup. Simulations reveal, that a stroboscopic diffraction echo scheme synchronized with the trap period is suitable for observing the expected long coherence times.

We also used Bragg spectroscopy for mapping the momentum distribution of the  ${}^6\text{Li}$  cloud. Details will be reported elsewhere. Differently from time-of-flight absorption imaging the resolution of this method is not limited by the imaging system, which may allow to resolve small scale features in the momentum distribution with high precision. Since the temperatures in our experiment are not deep in the Fermi regime, the integrated momentum distribution does not deviate much from that of an ultracold classical gas [16], such that we do not observe clear signatures of Fermi pressure.

Now shown to be applicable to fermions, Bragg spectroscopy may prove useful for probing distinct features of the dispersion relation such as rotons [17] or long-range many-body correlations such as Cooper-pairing or fermionic condensation [18]. In the future we aim to study the dynamical properties of heteronuclear spin mixtures with tunable interactions by performing Bragg scattering in the vicinity of one of the recently found heteronuclear Feshbach resonances [19]. Further, studies in the crossover regime from Bragg scattering to superradiance with fermions are planned [20].

This work has been supported by the Deutsche Forschungsgemeinschaft (DFG) within the Schwerpunktprogramm SPP1116. We acknowledge helpful discussions with Andreas Günther and Martin Zwierlein.

- 
- [1] M. Kozuma *et al.*, Phys. Rev. Lett. **82**, 871 (1999);
  - [2] J. Stenger *et al.*, Phys. Rev. Lett. **82**, 4569 (1999); J. Stenger *et al.*, Appl. Phys. B **69**, 347 (1999); D. M. Stamper-Kurn *et al.*, Phys. Rev. Lett. **83**, 2876 (1999); D. M. Stamper-Kurn and W. Ketterle, Les Houches 1999 Summer School, Session LXXII (2000); J. Steinhauer, R. Ozeri, N. Katz, and N. Davidson, Phys. Rev. Lett. **88**, 120407 (2002); J. Steinhauer *et al.*, Phys. Rev. Lett. **90**, 060404 (2003).
  - [3] J. R. Abo-Shaeer *et al.*, Phys. Rev. Lett. **94**, 040405 (2005).
  - [4] P. B. Blakie and R. J. Ballagh, J. Phys. B **33**, 3961 (2000); P. B. Blakie and R. J. Ballagh, Phys. Rev. Lett. **86**, 3930 (2001); S. R. Muniz, D. S. Naik, and C. Raman, Phys. Rev. A **73**, 041605(R) (2006).
  - [5] H. P. Büchler, P. Zoller, and W. Zwerger, Phys. Rev. Lett. **93**, 080401 (2004).
  - [6] J. E. Simsarian *et al.*, Phys. Rev. Lett. **85**, 2040 (2000); S. Inouye *et al.*, Nature **402**, 641 (1999).
  - [7] G. Roati, E. de Mirandes, F. Ferlaino, H. Ott, G. Modugno, and M. Inguscio, Phys. Rev. Lett. **92**, 230402 (2004)
  - [8] E. L. Hahn, Phys. Rev. **80**, 580 (1950).
  - [9] N. A. Kurnit, I. D. Abella, and S. R. Hartmann, Phys. Rev. Lett. **13**, 567 (1964).
  - [10] B. Golding and J. E. Graebner, Phys. Rev. Lett. **37**, 852 (1976).
  - [11] F. B. J. Buchkremer, R. Dumke, H. Levsen, G. Birkl,

- and W. Ertmer, Phys. Rev. Lett. **85**, 3121 (2000); E. Gershonabel *et al.*, Phys. Rev. A **69**, 041604(R) (2004).
- [12] C. Silber *et al.*, Phys. Rev. Lett. **95**, 170408 (2005).
- [13] In the decompressed trap,  $\omega_z/2\pi = 140.89$  Hz, we found dephasing times without  $^{87}\text{Rb}$  atoms exceeding 13 s, which is on the order of the magnetic trap lifetime.
- [14] C. Marzok, B. Deh, Ph. W. Courteille, and C. Zimmermann, Phys. Rev. A **76**, 052704 (2007).
- [15] M. F. Andersen, A. Kaplan, and N. Davidson, Phys. Rev. Lett. **90**, 023001 (2003).
- [16] B. DeMarco and D. S. Jin, Phys. Rev. A **58**, R4267 (1998).
- [17] J. Steinhauer, R. Ozeri, N. Katz, and N. Davidson, arXiv:cond-mat/0303375.
- [18] G. M. Bruun and G. Baym, Phys. Rev. A **74**, 033623 (2006); K. J. Challis, R. J. Ballagh, and C. W. Gardiner, Phys. Rev. Lett. **98**, 093002 (2007).
- [19] B. Deh, C. Marzok, C. Zimmermann, and Ph. W. Courteille, Phys. Rev. A **77**, 010701(R) (2008).
- [20] W. Ketterle and S. Inouye, Phys. Rev. Lett. **86**, 4203 (2001); L. Fallani *et al.*, Phys. Rev. A **71**, 033612 (2005).